A Temperature-Dependent Hysteresis Model for Relaxor Ferroelectric Compounds

Julie K. Raye * and Ralph C. Smith †

*Department of Mathematics, Virginia Commonwealth University, Richmond VA 23284-2014
†Center for Research in Scientific Computation, North Carolina State Univ., Raleigh, NC 27695

Abstract

This paper summarizes the development of a homogenized free energy model which characterizes the temperature-dependent hysteresis and constitutive nonlinearities inherent to relaxor ferroelectric materials. A kernel for the model is developed through mesoscopic energy analysis and extended to provide macroscopic constitutive relations through stochastic homogenization techniques based on the assumption that certain underlying parameters are manifestations of underlying densities rather than constants. Mechanisms characterizing the decrease in hysteresis and saturation polarization polarization as temperatures are increased are constructed using asymptotic properties of the kernel which is derived from statistical mechanics tenets. Attributes of the model are illustrated through comparison with PMN-PT-BT data.

Keywords: Hysteresis, relaxor ferroelectric compounds, constitutive nonlinearities materials

1. Introduction

Transducers employing relaxor ferroelectric materials are increasingly considered for applications ranging from sonar transduction to high precision optics due to their relatively large stroke capabilities and nearly anhysteretic behavior when employed within their diffuse transition region. However, the price paid for these superior performance capabilities is strong temperature-dependence in the dielectric properties of the materials. As illustrated by quasistatic PMN-PT-BT data in Figure 1, a decrease of 40^oC near the freezing temperature can lead from anhysteretic to hysteretic E-P relations with a significant increase in the saturation polarization. Since heat produced during transduction is proportional to the area of the hysteresis loop, materials operating in hysteretic regimes exhibit increased temperatures which subsequently reduces the hysteresis — this process proceeds until an equilibrium temperature is reached. To place the magnitude of these effects in perspective, we note that a PMN-driven flextensional sonar transducer submersed in water experiences a temperature increase of approximately 40^oC before equilibrium is reached [9]. Although less dramatic, similar mechanisms degrade the accuracy of relaxor-based nano- or micropositioners unless temperatures are carefully regulated. This motivates the development of comprehensive material models which characterize the temperature-dependent dielectric behavior in a manner which facilitates subsequent transducer design and model-based control implementation.

A number of the initial models for the relaxor ferroelectric compound lead magnesium niobate (PMN), and derivatives doped with lead titanate (PT), barium titanate (BT) and strontium titanate (ST), focused on the quantification of the anhysteretic behavior above the freezing temperature T_f — e.g., see [2, 3, 4, 5, 6]. Smith and Hom subsequently incorporated the hysteretic low-temperature behavior through the development of domain wall models having temperature-dependent coefficients [13, 14]. Whereas these models are very effective for symmetric loop behavior, they require *a priori* knowledge of turning points to guarantee biased minor loop closure which precludes their use in feedback control designs for transient dynamics.

*Email: jkraye@vcu.edu; Telephone: 804-828-1301x375
†Email: rsmith@eos.ncsu.edu; Telephone: 919-515-7552

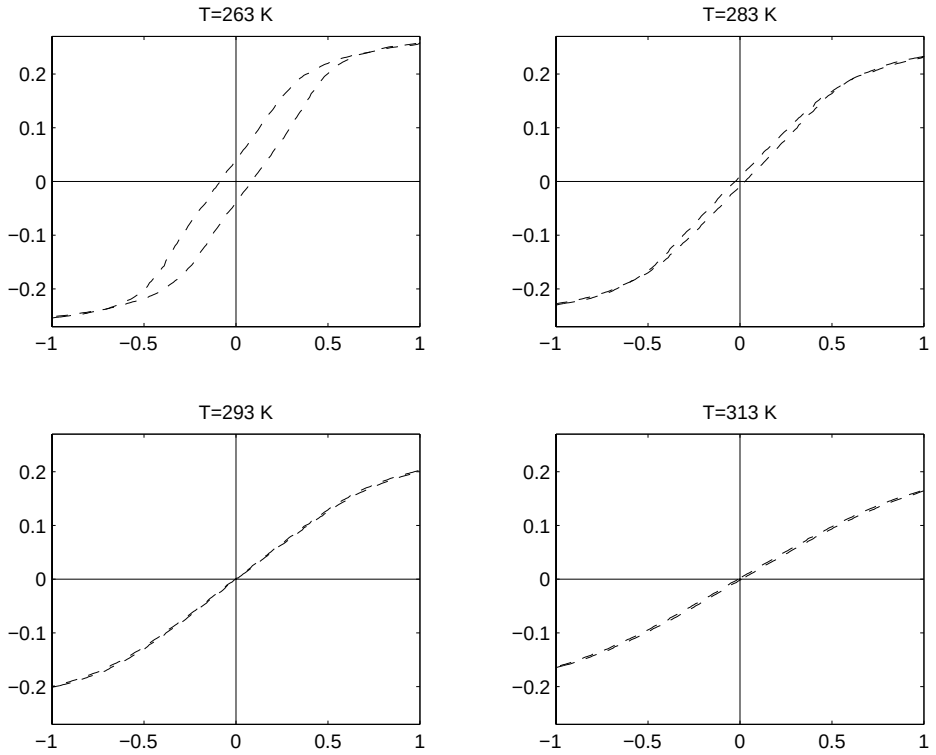

Figure 1: Decreasing hysteresis and saturation polarization of PMN-PT-BT as a function of increasing temperature (from [13, 14]).

In this paper, we extend the homogenized free energy framework, developed in [17] for ferroelectric materials, to incorporate temperature effects inherent to relaxor ferroelectric compounds. In Section 2, we summarize the previous fixed-temperature model which is comprised of an energy-based kernel derived at the mesoscopic level with macroscopic effective parameters determined through stochastic homogenization techniques. Thermodynamic properties of the kernel are exploited in Section 3 to construct mechanisms that incorporate the temperature-dependent behavior illustrated in Figure 1. Attributes of the model are illustrated in Section 4 through a comparison with quasistatic PMN-PT-BT data.

2. Isothermal Hysteresis Model

To provide the framework for incorporating temperature-dependent behavior, we summarize first the hysteresis model developed in [17] for ferroelectric materials.

2.1. Helmholtz and Gibbs Energies

As detailed in [17], combination of the internal energy derived under the assumption that dipoles align either with the applied field, or diametrically opposite to it, and classical entropy relations yields the temperature-dependent Helmholtz energy relation

$$\psi(P,T) = \frac{E_h P_s}{2}\left[1-(P/P_s)^2\right] + \frac{E_h T}{2T_c}\left[P\ln\left(\frac{P+P_s}{P_s-P}\right) + P_s\ln(1-(P/P_s)^2)\right]. \tag{1}$$

Here E_h, T_c and P_s respectively denote a bias field, the Curie temperature and the saturation polarization. It can be easily verified that (1) incorporates double well behavior for $T < T_c$ and a single potential well for

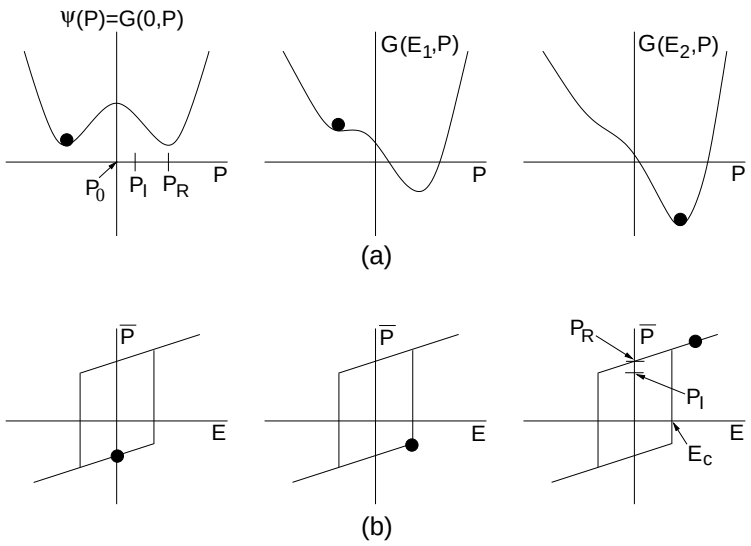

Figure 2: (a) Helmholtz energy ψ and Gibbs energy G for increasing field E ($E_2 > E_1 > 0$). (b) Dependence of the local average polarization $\overline{P}$ on the field E.

$T > T_c$ in accordance with the ferroelectric to paraelectric phase transition associated with materials exhibiting second-order phase transitions.

Whereas derived from statistical mechanics tenets, the Helmholtz relation (1) is often better suited for qualitative rather than quantitative characterization due to the restricted assumptions leading to its formulation. To provide additional flexibility and efficiency in fixed-temperature regimes, a second choice for the Helmholtz functional is the piecewise quadratic construct

$$\psi(P) = \begin{cases} \frac{1}{2}\eta(P + P_R)^2 & , \ P \leq -P_I \\ \frac{1}{2}\eta(P - P_R)^2 & , \ P \geq P_I \\ \frac{1}{2}\eta(P_I - P_R)\left(\frac{P^2}{P_I} - P_R\right) & , \ |P| < P_I \end{cases} \tag{2}$$

which can be interpreted as being derived through Taylor expansions at each of the equilibria of (1). As illustrated in Figure 2, P_I and P_R respectively denote the inflection point and polarization at which the minimum of ψ occurs.

Recalling that the electrostatic energy is given by $U_E = -\mathbf{p} \cdot \mathbf{E}$, where $\mathbf{p}$ is a dipole in an electric field $\mathbf{E}$, we construct the Gibbs energy relation

$$G = \psi - EP \tag{3}$$

where ψ is given by (2) or (3). The behavior of G for increasing fields is illustrated in Figure 2(a).

2.2. Local Polarization Relation for Negligible Thermal Activation

For operating regimes in which thermal activation is negligible and relaxation times are small compared with drive frequencies, the local average polarization $\overline{P}$ is determined directly the minimization of the Gibbs energy (3). For the Helmholtz relation (1), enforcement of the necessary condition $\frac{\partial G}{\partial P} = 0$ yields

$$\overline{P}(E) = P_s \tanh\left(\frac{E + \alpha P}{a(T)}\right)$$

where $\alpha = \frac{E_h}{P_s}$ and $a(T) = \frac{E_h T}{T_c}$. The kernel resulting from the piecewise quadratic relation (2) has the general form

$$\overline{P}(E) = \frac{1}{\eta}E + P_R\delta \tag{4}$$

where $\delta = -1$ for negatively oriented dipoles and $\delta = 1$ for those with positive orientation. To specify δ and hence $\overline{P}$ more specifically in terms of the initial dipole orientations and previous switches, we employ the Preisach notation and take

$$[\overline{P}(E;E_c,\xi)](t) = \begin{cases} [\overline{P}(E;E_c,\xi)](0) & , \tau(t) = \emptyset \\ \frac{E}{\eta} - P_R & , \tau(t) \neq \emptyset \text{ and } E(\max\tau(t)) = -E_c \\ \frac{E}{\eta} + P_R & , \tau(t) \neq \emptyset \text{ and } E(\max\tau(t)) = E_c \end{cases} \tag{5}$$

where

$$[\overline{P}(E;E_c,\xi)](0) = \begin{cases} \frac{E}{\eta} - P_R & , E(0) \leq -E_c \\ \xi & , -E_c < E(0) < E_c \\ \frac{E}{\eta} + P_R & , E(0) \geq E_c \end{cases}$$

defines the initial states of the kernel. The local coercive field

$$E_c = \eta(P_R - P_I) \tag{6}$$

quantifies the field at which the negative well ceases to exist and hence a dipole switch occurs. Finally, if t_f designates the final time under consideration, the set of switching times is given by

$$\tau(t) = \{t \in (0,t_f] \,|\, E(t) = -E_c \text{ or } E(t) = E_c\}.$$

The behavior of the piecewise linear hysteron (4) or (5) is illustrated in Figure 2(b), and this is the kernel we consider throughout the remainder of the development.

2.3. Local Polarization Relation Incorporating Thermal Activation

To include the effects of thermal relaxation, it is necessary to balance the Gibbs energy G with the relative thermal energy kT/V, where k and V respectively denote Boltzmann's constant and a reference volume, through the Boltzmann relation

$$\mu(G) = Ce^{-GV/kT}.$$

The constant C is specified to guarantee integration to unity when considered over all admissible dipole orientations.

The local average polarization in this case is given by

$$\overline{P} = x_+ \langle P_+ \rangle + x_- \langle P_- \rangle \tag{7}$$

where x_+ and x_- respectively denote the fractions of dipoles having positive and negative orientations and $\langle P_+ \rangle, \langle P_- \rangle$ are the associated average polarizations. As detailed in [17], the latter are quantified by the general relations

$$\langle P_+ \rangle = \int_{P_I}^{\infty} P\mu(G)\,dP \quad , \quad \langle P_- \rangle = \int_{-\infty}^{-P_I} P\mu(G)\,dP.$$

Evaluation of the integration constant subsequently yields

$$\langle P_+ \rangle = \frac{\displaystyle\int_{P_I}^{\infty} Pe^{-G(E,P)V/kT}dP}{\displaystyle\int_{P_I}^{\infty} e^{-G(E,P)V/kT}dP} \quad , \quad \langle P_- \rangle = \frac{\displaystyle\int_{-\infty}^{-P_I} Pe^{-G(E,P)V/kT}dP}{\displaystyle\int_{-\infty}^{-P_I} e^{-G(E,P)V/kT}dP}.$$

The evolution of dipole fractions are quantified by the differential equations

$$\dot{x}_+ = -p_{+-}x_+ + p_{-+}x_-$$
$$\dot{x}_- = -p_{-+}x_- + p_{+-}x_+$$

which can be simplified to

$$\dot{x}_+ = -p_{+-}x_+ + p_{-+}(1 - x_+)$$

through the identity $x_+ + x_- = 1$. Here

$$p_{+-} = \frac{1}{\mathcal{T}(T)} \frac{\displaystyle\int_{P_I-\epsilon}^{P_I} e^{-G(E,P)V/kT} dP}{\displaystyle\int_{P_I-\epsilon}^{\infty} e^{-G(E,P)V/kT} dP} \quad , \quad p_{-+} = \frac{1}{\mathcal{T}(T)} \frac{\displaystyle\int_{-P_I}^{-P_I+\epsilon} e^{-G(E,P)V/kT} dP}{\displaystyle\int_{-\infty}^{-P_I+\epsilon} e^{-G(E,P)V/kT} dP} \tag{8}$$

respectively denote the likelihoods that dipoles switch from positive to negative, and conversely. In (8), ϵ is a small positive constant and $\mathcal{T}$ denotes the material-dependent relaxation time. As detailed in [17], the local average polarization relation (7) converges to the piecewise linear relation (5) in the limit $kT/V \to 0$ of negligible relative thermal energy.

2.4. Macroscopic Polarization Model

The local polarization relations (5) and (7) are derived under the assumption of a uniform lattice and effective field. Hence they provide adequate approximations for certain single crystal compounds but neglect the effects of polycrystallinity, material and stress nonhomogeneities, and variable effective fields which contribute significantly to the hysteretic behavior of general polycrystalline compounds. We incorporate these effects by considering the local coercive and effective fields to be manifestations of underlying distributions rather than constants. This provides low-order macroscopic polarization employing the relations (5) or (7) as a kernel.

It is demonstrated in [17] that distributed coercive and effective field behavior can be incorporated through the general formulation

$$[P(E)](t) = \int_0^{\infty} \int_{-\infty}^{\infty} \nu_1(E_c)\nu_2(E_e)[\overline{P}(E_e + E; E_c, \xi)](t)\, dE_e\, dE_c \tag{9}$$

where $\overline{P}$ is given by (5) or (7). The densities ν_1 and ν_2 characterizing the coercive and effective field distributions must satisfy certain physical decay criteria but otherwise can be considered to be general. Details regarding the formulation of the model and identification techniques for estimating the general densities can be found in [10, 12].

Alternatively, one can consider parametric forms for the densities which satisfy the constraint that the coercive field is positive and both densities exhibit exponential decay. In this latter vein, we consider the choices

$$\begin{aligned} \nu_1(E_c) &= c_1 e^{-[\ln(E_c/\overline{E}_c)/2c]^2} \\ \nu_2(E_e) &= c_2 e^{-E_e^2/b}. \end{aligned} \tag{10}$$

It is established in [1] that if c is small compared with $\overline{E}_c$, the norm and variance for the lognormal distribution have the approximate values

$$\langle E_c \rangle \approx \overline{E}_c \quad , \quad \sigma \approx 2\overline{E}_c\, c\,.$$

These relations can be employed to obtain initial parameter estimates which reflect properties of the measured data. In the next section, we detail the modifications required to incorporate temperature-dependence in the densities (10) and hence the polarization model (9).

3. Thermal Hysteresis Model

Because the Helmholtz relation (1) was constructed through a balance of internal energy and relative entropy over a representative volume, it encapsulates the diminishing hysteresis observed in materials exhibiting second-order phase transitions as temperatures are increased through the Curie point. However, its applicability for characterizing general temperature-dependent behavior of the type illustrated in Figure 1 should be considered

as qualitative rather than quantitative due to the restricted assumptions underlying its formulation. Instead, we use it to predict extensions to the piecewise quadratic functional (2) to incorporate relevant temperature-dependencies.

3.2. Model Formulation

Analysis of the data in Figure 1 indicates that as temperatures are increased through the freezing temperature T_f, the local coercive field E_c, local remanence value P_R and inflection point P_I all decrease. We focus first on the latter.

For the Helmholtz energy relation (1), the inflection point P_I is determined by $\frac{\partial^2 G}{\partial P^2} = 0$ where G is given (2). Since

$$\frac{\partial^2 G}{\partial P^2} = \frac{-E_h}{P_s} + \frac{E_h T}{T_c P_s} \frac{1}{1-(P/P_s)^2},$$

this yields

$$\pm P_I(T) = \pm P_s \sqrt{1 - T/T_c}.$$

Because the coercive field E_c is the point at which dipole switches occur, it follows that

$$\begin{aligned} E_c(T) &= \frac{E_h}{P_s} P_I(T) - \frac{E_h T}{T_c} \text{arctanh}(P_I(T)/P_s) \\ &= E_h \sqrt{1 - T/T_c} - \frac{E_h T}{T_c} \text{arctanh} \sqrt{1 - T/T_c} \\ &= E_h \sqrt{1 - T/T_c} - \frac{E_h T}{T_c} \left[\sqrt{1 - T/T_c} + \frac{1}{3}(1 - T/T_c)^{3/2} + \ldots \right] \\ &= E_h (1 - T/T_c)^{3/2} \left[1 - \frac{1}{3}\frac{T}{T_c} + \ldots \right]. \end{aligned} \tag{11}$$

Finally, through the relation (6), the local remanence polarization

$$\begin{aligned} P_R(T) &= \frac{E_c(T)}{\eta} + P_I(T) \\ &= \frac{E_h}{\eta}(1 - T/T_c)^{3/2} \left[1 - \frac{1}{3}\frac{T}{T_c} + \ldots \right] + P_s \sqrt{1 - T/T_c} \end{aligned} \tag{12}$$

inherits temperature-dependence from both E_c and P_I.

We generalize the expansions in (11) and (12) to obtain

$$\overline{E}_c(T) = E_h (1 - T/T_c)^p$$

and

$$P_R(T) = \frac{E_h}{\eta}(1 - T/T_c)^p + P_s (1 - T/T_c)^q.$$

The temperature-dependent coercive field is employed in the density ν_1 of (10) and the temperature-dependent remanence value is incorporated in the linear kernel $\overline{P}$ given by (4) or (7).

3.2. Model Implementation

To implement the model (9), it is necessary to approximate the integrals in a manner which is sufficiently efficient to permit eventual real-time control implementation. We accomplish this by discretizing the integrals via a composite Gaussian quadrature rule followed by development of a highly efficient matrix algorithm for evaluating the `if-then` constructs encapsulated in the kernel definitions (4) or (5). Details regarding these algorithms can be found in [17].

The assumption that densities exhibit exponential decay permits us to truncate the domain. A composite Gaussian quadrature discretization on the resulting compact support yields the approximate polarization model

$$[P(E,T)](t) = \sum_{i=1}^{N_i}\sum_{j=1}^{N_j}[\overline{P}(E_{e_j}+E;E_{c_i},\xi_j)](t)e^{-E_{e_j}^2/b}e^{-[\ln(E_{c_i}/\overline{E}_c(T)/2c]^2}v_iw_j \tag{13}$$

where E_{e_j}, E_{c_i} denote the abscissas associated with respective quadrature formulae and v_i, w_j are the respective weights — e.g., see pages 698–699 of [18].

We now provide details illustrating the evaluation of the kernel $[\overline{P}(E_{e_j}+E,E_{c_i},\xi_i)](t)$. The crux of the algorithm entails the determination of the active kernel branch indicated by (5) while avoiding the inefficiency inherent to direct evaluation of `if-then` statements. To motivate the algorithm, we suppose that we want to find the polarization corresponding to the effective field $E = E(t_k) + E_e$ at the k^{th} time step for a fixed variation E_e and coercive field E_c. If the polarization at the previous $(k-1)^{th}$ time step is on the positive branch, then $P(E_k)$ is on the positive branch if $E-(-E_c)$ is positive and on the negative branch if $E-(-E_c)$ is negative. If $P(E_{k-1})$ is on the negative branch, then $P(E_k)$ is on the negative branch if $E-E_c$ is negative and on the positive branch if $E-E_c$ is positive. Hence the polarization at $P(E_k)$ depends on $E+E_c$ if $P(E_{k-1})$ is on the positive branch and $E+E_c$ if $P(E_{k-1})$ is on the negative branch. Thus, we are interested in the quantity

$$\Delta = \text{sign}(E + \Delta_0 E_c)$$

where Δ_0 denotes the polarization branch at the previous time step and

$$\text{sign}(x) = \begin{cases} 1, & x > 0 \\ 0, & x = 0 \\ -1, & x < 0\,. \end{cases}$$

We now use Δ in an algorithm to compute $\overline{P}$. We begin by defining the matrices

$$\hat{E}_c = \begin{bmatrix} E_{c_1} & \cdots & E_{c_1} \\ \vdots & & \vdots \\ E_{c_{N_i}} & \cdots & E_{c_{N_i}} \end{bmatrix}_{N_i\times N_j} \qquad \hat{E}_e = \begin{bmatrix} E_k+E_{e_1} & \cdots & E_k+E_{e_{N_j}} \\ \vdots & & \vdots \\ E_k+E_{e_1} & \cdots & E_k+E_{e_{N_j}} \end{bmatrix}_{N_i\times N_j}$$

$$\Delta_0 = \begin{bmatrix} -1 & \cdots & -1 & 1 & \cdots & 1 \\ \vdots & & \vdots & \vdots & & \vdots \\ -1 & \cdots & -1 & 1 & \cdots & 1 \end{bmatrix}_{N_i\times N_j}.$$

and weight vectors

$$W^T = \begin{bmatrix} w_1e^{-E_{e_1}^2/b} & \cdots & w_{N_j}e^{-E_{e_{N_j}}^2/b} \end{bmatrix}_{1\times N_j}$$
$$V^T = \begin{bmatrix} v_1e^{-[\ln(E_{c_1}/\overline{E}_c)/2c]^2} & \cdots & v_{N_i}e^{-[\ln(E_{c_{N_i}}/\overline{E}_c)/2c]^2} \end{bmatrix}_{1\times N_i}.$$

At each time step we compute $\overline{P} = \frac{1}{\eta}\hat{E}_e + P_R\Delta$ and use these values to calculate the matrix Δ as given by

$$\Delta = \text{sign}(\hat{E}_e + \Delta_0\hat{E}_c).$$

Finally, we update

$$\overline{P} = \frac{1}{\eta}\hat{E}_e + \Delta P_R$$
$$\Delta_0 = \Delta$$

and perform the matrix-vector multiplication

$$P = CV^T\overline{P}W$$

to compute the sum.

4. Experimental Validation

To illustrate the performance of the temperature-dependent hysteresis model, we use it to characterize the PMN-PT-BT behavior plotted in Figure 1. To construct the model, it is necessary to estimate the parameters

$$q = [E_h, T_c, P_s\eta, c, b, \frac{C}{\eta}, p, q]^T$$

through a least squares fit to the data. To designate a least squares functional, we let $\{\widehat{E}_k, \widehat{P}_k\}$, $k = 1, \ldots, N_d$, denote the combined data collected at four temperatures, 263, 278, 293, and 313, and define parameter-dependent solutions to (13) by $P(\widehat{E}_k, T; q)$. The least squares functional

$$J(q) = \sum_{k=1}^{N_d} |P(\widehat{E}_k, T; q) - \widehat{P}_k|^2$$

was then minimized using the Matlab simplex algorithm `fmins.m` to obtain the parameter values $T_c = 330.8$ K, $E_h = 7.5 \times 10^5$ Mv/m, $b = 2.1 \times 10^{11}$, $P_s\eta = 6.0275$ (C/m^2)(MVm/C), $\frac{C}{\eta} = 10^{-7}$ C/MVm, $c = 0.16$, $p = 1.4$, and $q = 0.85$.

The resulting model fit is compared with the quasistatic (collected at 1 Hz) PMN-PT-BT data in Figure 3. It is observed that the model accurately characterizes the diminishing hysteresis and saturation polarization values measured in the material as temperatures are increased within the diffuse transition region. Hence it provides an initial framework quantifying temperature-dependent relaxor ferroelectric behavior of transducer design and model-based control implementation.

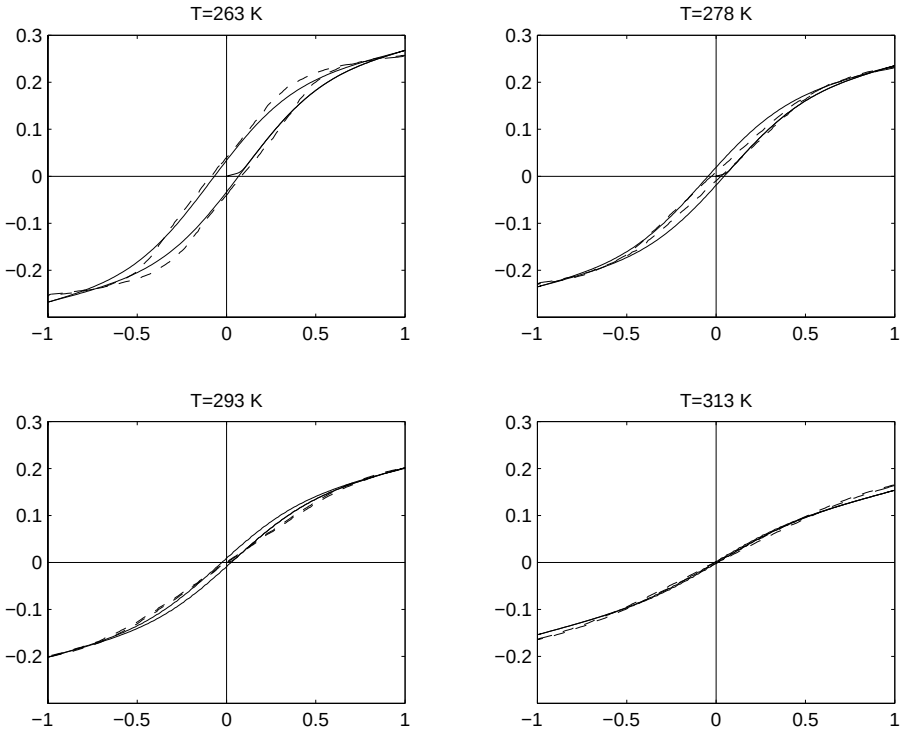

Figure 3: PMN-PT-BT data (– – –) and homogenized free energy model (——). Abscissas: electric field (MV/m), ordinates: polarization (C/m^2).

5. Concluding Remarks

The model developed here extends the framework in [17] to incorporate temperature-dependent hysteresis and nonlinear constitutive behavior inherent to relaxor ferroelectric compounds. Specifically, it employs asymptotic properties of an underlying mesoscopic kernel constructed using mean field theory to incorporate mechanisms which provide the decrease in hysteresis and saturation polarization measured in relaxors as temperatures are increased within the diffuse transition region.

The underlying framework provides a number of properties which make it advantageous for material characterization, transducer design, and model-based control design. As detailed in [17], the framework provides reversibility and guarantees closure of biased minor loops. It also provides an energy basis for certain extended Preisach models [15] and establishes a unified framework for characterizing hysteresis and constitutive nonlinearities in ferroelectric, ferromagnetic and ferroelastic materials. Finally, the fact that it can be efficiently inverted provides the capability for constructing inverse filters for linear feedback or feedforward control designs [7, 8, 11].

Acknowledgements

This research was supported through the NSF grant CMS-009764 and the Air Force Office of Scientific Research under the grant AFOSR-F49620-01-1-0107.

References

Note: Center for Research in Scientific Computation Technical Reports can be accessed at the web site `http://www.ncsu.edu/crsc/reports.html`.

[1] E. Della Torre, *Magnetic Hysteresis*, IEEE Press, New York, 1999.

[2] A.E. Glazounov, A.J. Bell and A.K. Tagantsev, "Relaxors as superparaelectrics with distributions of the local transition temperature," *Journal of Physics: Condensed Matter*, 7(21), pp. 4145–4168, 1995.

[3] C.L. Hom, P.D. Dean and S.R. Winzer, "Simulating electrostrictive deformable mirrors: I. Nonlinear static analysis," *Smart Materials and Structures* 8, pp. 691–699, 1999.

[4] C.L. Hom and N. Shankar, "A fully coupled constitutive model for electrostrictive ceramic materials," *Journal of Intelligent Material Systems and Structures*, 5, pp. 795–801, 1994.

[5] C.L. Hom and N. Shankar, "Modeling nonlinearity in electrostrictive sonar transducers," *Journal of the Acoustical Society of America*, 104(4), pp. 1903–1913, 1998.

[6] C.L. Hom and N. Shankar, "A constitutive model for relaxor ferroelectrics," Proceedings of the SPIE, Smart Structures and Materials 1999, Volume 3667, pp. 134–144, 1999.

[7] J.M. Nealis and R.C. Smith, "$\mathcal{H}_\infty$ Control Design for a Magnetostrictive Transducer," Proceedings of the 42nd IEEE Conference on Decision and Control, Maui, HA, pp. 1801-1806, 2003.

[8] J.M. Nealis and R.C. Smith, "Model-Based Robust Control Design for Magnetostrictive Transducers Operating in Hysteretic and Nonlinear Regimes," CRSC Technical Report CRSC-TR03-25; *IEEE Transactions on Automatic Control*, submitted.

[9] N. Shankar and C.L. Hom, "An acoustic/thermal model for self-heating in PMN sonar projectors," *Journal of the Acoustical Society of America*, submitted.

[10] R.C. Smith and A. Hatch, "Parameter estimation techniques for nonlinear hysteresis models," Proceedings of the SPIE, Smart Structures and Materials 2004, to appear.

[11] R.C. Smith, A. Hatch and T. De, "Model Development for Piezoceramic Nanopositioners," Proceedings of the 42nd IEEE Conference on Decision and Control, Maui, HA, pp. 2638-2643, 2003.

[12] R.C. Smith, A. Hatch, B. Mukherjee and S. Liu, "A homogenized energy model for hysteresis in ferroelectric materials: General density formulation," preprint.

[13] R.C. Smith and C.L. Hom, "A temperature-dependent hysteresis model for relaxor ferroelectrics," Proceedings of the SPIE, Smart Structures and Materials 2000, Newport Beach, CA, Volume 3992, pp. 267–278, 2000.

[14] R.C. Smith and H.L. Hom, "A temperature-dependent constitutive model for relaxor ferroelectrics," CRSC Technical Report CRSC-TR00-26; *Journal of Intelligent Material Systems and Structures*, submitted.

[15] R.C. Smith and S. Seelecke, "An energy formulation for Preisach models," Proceedings of the SPIE, Smart Structures and Materials 2002, Volume 4693, pp. 173–182, 2002.

[16] R.C. Smith, S. Seelecke and Z. Ounaies, "A free energy model for piezoceramic materials," Proceedings of the SPIE, Smart Structures and Materials 2002, Volume 4693, pp. 183-190, 2002.

[17] R.C. Smith, S. Seelecke, Z. Ounaies and J. Smith, "A free energy model for hysteresis in ferroelectric materials," *Journal of Intelligent Material Systems and Structures*, 14(11), pp. 719–739, 2003.

[18] D. Zwillinger, Editor-in-Chief, *CRC Standard Mathematical Tables and Formulae*, 30th Edition, CRC Press, Boca Raton, 1996.